Published in final edited form as:
J Neurol Sci. 2009 July 15; 282(1-2): 39–46. doi:10.1016/j.jns.2008.12.035.

Deep Gray Matter Atrophy in Multiple Sclerosis: A Tensor Based Morphometry

Guozhi Tao[1], **Sushmita Datta**[1], **Renjie He**[1], **Flavia Nelson**[2], **Jerry S. Wolinsky**[2], and **Ponnada A. Narayana**[1,*]

[1]Department of Diagnostic and Interventional Imaging, University of Texas Medical School at Houston, 6431 Fannin Street, Houston, TX 77030

[2]Department of Neurology, University of Texas Medical School at Houston, 6431 Fannin Street, Houston, TX 77030

Abstract

Tensor based morphometry (TBM) was applied to determine the atrophy of deep gray matter (DGM) structures in 88 relapsing multiple sclerosis (MS) patients. For group analysis of atrophy, an unbiased atlas was constructed from 20 normal brains. The MS brain images were co-registered with the unbiased atlas using a symmetric inverse consistent nonlinear registration. These studies demonstrate significant atrophy of thalamus, caudate nucleus, and putamen even at a modest clinical disability, as assessed by the expanded disability status score (EDSS). A significant correlation between atrophy and EDSS was observed for different DGM structures: (thalamus: $r = -0.51$, $p = 3.85\times10^{-7}$; caudate nucleus: $r = -0.43$, $p = 2.35\times10^{-5}$; putamen: $r = -0.36$, $p = 6.12\times10^{-6}$). Atrophy of these structures also correlated with 1) T2 hyperintense lesion volumes (thalamus: $r = -0.56$, $p = 9.96\times10^{-9}$; caudate nucleus: $r = -0.31$, $p = 3.10\times10^{-3}$; putamen: $r = -0.50$, $p = 6.06\times10^{-7}$), 2) T1 hypointense lesion volumes (thalamus: $r = -0.61$, $p = 2.29\times10^{-10}$; caudate nucleus: $r = -0.35$, $p = 9.51\times10^{-4}$; putamen: $r = -0.43$, $p = 3.51\times10^{-5}$), and 3) normalized CSF volume (thalamus: $r = -0.66$, $p = 3.55\times10^{-12}$; caudate nucleus: $r = -0.52$, $p = 2.31\times10^{-7}$, and putamen: $r = -0.66$, $p = 2.13\times10^{-12}$). More severe atrophy was observed mainly in thalamus at higher EDSS. These studies appear to suggest a link between the white matter damage and DGM atrophy in MS.

Keywords

multiple sclerosis; atrophy; deep gray matter structures; inverse consistent nonlinear registration; tensor based morphometry

1. Introduction

Multiple sclerosis (MS) is the most common central nervous system demyelinating disease in humans. Approximately 85−90% of the MS population falls into the relapsing remitting (RR) phenotype [1]. Although traditionally MS is considered to be a white matter (WM) disease,

*__Corresponding Author__ Department of Diagnostic and Interventional Imaging University of Texas Medical School at Houston 6431 Fannin Street Houston, TX 77030 Phone: (713)500−7677 Fax: (713)500−7684 Email: ponnada.a.narayana@uth.tmc.edu.

pathology studies dating back to the 19th century identified gray matter (GM) involvement in MS [2,3] and further elaborated by detailed histopathology in 1916 [4]. Recent studies with sensitive immunohistochemical techniques confirm a high prevalence of cortical lesions and suggest that cortical involvement may be diffuse or highly localized, with relatively minimal inflammation [5-7]. Cortical GM involvement in MS has also been demonstrated by MRS [8-12], MTR [13-15], and DTI [16-20]. Based on various MR measures, the deep gray matter (DGM) is also affected in MS [21-28]. Significant neurodegeneration and volume loss in thalamus have been reported in MS [26,29]. Both thalamus and putamen atrophy have been reported in clinically isolated syndrome [30]. Caudate atrophy has been demonstrated on MRI and was shown to correlate with cognitive deficit [31] and used as a marker for GM loss in aging and various neurological disorders [32]. Caudate atrophy is also consistent with hypometabolism on positron emission tomography (PET) and appears to correlate with fatigue in MS [33].

DGM atrophy has also been shown to occur early on in the disease course in MS and appears to correlate better with clinical disability, including cognitive deficits, than with T2 lesion load [30,34-40]. DGM atrophy appears to be disproportionately high compared to the whole brain atrophy [21,29]. It has been suggested that regional atrophy associated with various DGM structures may be a valid biomarker in clinical trials [41].

There is a general agreement about the presence of DGM atrophy. However, there does not appear to be a consensus about the correlation between DGM atrophy and other MRI-derived measures and expanded disability status scale (EDSS). Bakshi et al. [42] reported that the regional brain atrophy and T2 lesion load are associated with EDSS. However, others found correlation between DGM atrophy with T2 lesion load, but not with EDSS [43,44]. Most of the studies reported that thalamus is predominantly atrophied in MS and is correlated with EDSS, T2 hyperintense (here used to designate the MRI-defined lesion volume that excludes the black hole or T1 hypointense component), T1 hypointense lesions, and brain atrophy [29, 30,35,45]. Bermel et al., 2003 [21] have reported caudate nucleus atrophy in MS but did not find any correlation with T1 or T2 lesion burden. In contrast, Prinster et al. [43] observed a correlation between caudate nucleus atrophy and lesion burden. Henry et al. [30] reported a correlation between putamen atrophy and clinical disability, as assessed by MS functional composite (MSFC) [46,47].

Much of the earlier work on regional atrophy was based on manual or semiautomatic segmentation [21,29]. However, more recently, voxel based morphometry (VBM) [48,49] is used for robust estimation of atrophy in MS [30,35,43-45,50]. In VBM, all individual anatomical images are spatially normalized to a common stereotactic space, which are then segmented into different tissue classes followed by smoothing of each tissue map [48]. The volume changes in tissue maps of individual brains are corrected by multiplying tissue voxel values by their respective Jacobian determinants (JDs) obtained from the spatial normalization step [49]. This technique allows group analysis in an automated way without the need to define *a priori* the structures of interest.

Tensor-based morphometry (TBM) is a more recent technique for estimating disease-related changes in brain structures and has been shown to provide methodological improvements over VBM. Jacobian determinant is one of the major TBM metrics that can directly measure tissue growth and atrophy [51]. The main advantage of TBM over VBM is that the former can be applied directly on the JDs of deformation fields without the need for tissue segmentation [41,52]. Whitford et al. [53] have used TBM to assess volumes of WM in first-episode schizophrenia. Brambati et al. [54-55] have applied TBM to monitor the progress of atrophy in semantic dementia. TBM is also currently used in the analysis of brain structures in traumatic brain injury [52], Alzheimer's disease [41,56-57], and HIV/AIDS [58]. Both VBM and TBM

require the use of a template or atlas for volume changes relative to a comparison group. The use of unbiased atlas as the template against which the volume changes are measured is thought to be more robust against registration errors and improves statistical power [52,59-60].

In this study, we applied TBM [57,61-62] for determining the atrophy of GM, with a particular emphasis on DGM structures. A symmetric nonlinear registration algorithm [63] was used to generate the geometric mean population or unbiased template. The statistical analysis for investigating various group differences was performed with SPM2 software package [48]. The regional volume changes in the GM structures were calculated as the average logarithm of JD maps of the deformation fields. The correlations between atrophy of GM structures and EDSS, T2 hyperintense and T1 hypointense lesion loads, and normalized CSF (nCSF) (a measure of whole brain atrophy) were investigated. In addition, the progression of atrophy with EDSS was examined.

2. Methods

2.1 Patients and MR Image Acquisition

A total of 88 relapsing MS patients, 68 females and 20 males, were recruited for this study. Their median age was 41.2 yrs (range: 20−64 yrs) with a median EDSS of 1.5 (range: 0−6.5). The diagnosis was confirmed by retrospective chart review (JSW), using the criteria of McDonald as revised in 2005 [64]. The EDSS was assessed by neurologists prior to or shortly after the time of performance of the MRI scans. None of the subjects had received corticosteroids within 30 days of imaging. At the time of imaging 22% of subjects were on no disease modifying therapy, the others were taking either glatiramer acetate (60%) or an interferon beta preparation (18%). The frequency distribution of EDSS in this patient population is shown in Table 1. This study was approved by our institution's Committee for the Protection of Human Subjects and is fully HIPAA compliant. Written informed consent was obtained from each patient.

All patients were scanned on a 3T Philips Intera scanner (Philips Medical Systems, Best, Netherlands) with a gradient system capable of producing a maximum gradient amplitude of 80 mT/m with a slew rate of 200 T/m/s. The MRI protocol included the following sequences: 1) dual fast spin echo (FSE) with TE1/TE2/TR: 9.5 ms/90 ms/6800 ms; 2) fluid attenuation inversion recovery (FLAIR) with TE/TR/TI: 80 ms/10000 ms/2600 ms; 3) pre- and post-contrast T1-weighted spin echo with TE/TR = 9.2/600 ms; and 4) 3D T1-weighted images either using fast field echo sequence (TE/TR = 4.6 ms/9.9 ms; 77 patients) or with magnetization prepared rapid gradient echo (MPRAGE) sequence (TE/TR = 3.7 ms/8.1 ms; 11 patients). Here TE, TR, and TI represent the echo, repetition, and inversion times, respectively. All images were acquired with a field-of-view 240 mm × 240 mm, image matrix of 256 × 256. Contiguous dual echo FSE, FLAIR images, pre- and post-contrast T1-weighted spin echo covering the whole brain, were acquired with slice thickness 3 mm and 3D T1-weighted images were acquired with a slice thickness of 1mm.

For the unbiased template construction, high resolution T1-weighted brain images from normal volunteers (45.2 ± 9.0 yrs) were obtained from the OASIS database [65]. The individual T1 image volume (MNI template, Colin 27) and associated anatomical labels were obtained from the UCLA website: http://www.loni.ucla.edu/Atlases.

2.2 Image Preprocessing

Dual echo FSE and FLAIR images were co-registered using the 3D rigid body registration. The extrameningeal tissues were removed (brain stripping) in the FSE, FLAIR and the 3D T1 images using the in-house developed semi-automated software. Bias field correction was

applied to minimize intensity nonuniformities using the module in the statistical parametric mapping (SPM2) software package [66].

2.3 Creation of Unbiased Template

The randomly selected 20 high-resolution T1 images of normal brains from the OASIS database [64] were used to construct an unbiased template [41,59] using a nonlinear registration algorithm [63]. We have used high resolution T1 images (MNI template) and associated anatomical labels to automatically identify and localize various anatomical structures in each of the MS brains. The symmetric cost function for the nonlinear registration algorithm was constructed to guarantee inverse consistency for morphometric measurements. An alternative minimization approach [67] was used to minimize different terms to avoid difficulties in balancing divergent terms, such as similarity measure, regularization of the transformation, and inverse consistent error. Mutual information (MI) was employed as the similarity measure and the dense MI flow was used as the external force for driving the registration process to deal with the intensity variations in different image volumes. Diffeomorphic mapping was achieved by updating the displacement fields through the composition scheme [63].

The major steps in the creation of unbiased template are shown in Figure 1. The 20 normal brains from OASIS datasets (two of the 20 images are shown in Figs. 1A and 1B) were registered to the MNI template (Fig. 1C). The intensity of all the deformed images were averaged to obtained the intensity averaged image in the MNI space (Fig. 1D). The geometric average of the transformation fields of the 20 co-registered images was obtained by averaging the transformations defined on the grid points of the MNI template. Since the JD of the geometric average transformation was found to be positive for all voxels (Fig. 1E), the unbiased template [41] was obtained by mapping the averaged image in the MNI space through inversion of the geometric average transformation (defined on the grid points of geometric average space) [68] (Fig.1F).

2.4 TBM analysis

Initially the 3D T1 images obtained on the 88 MS subjects were registered to the unbiased template with 12 parameter affine registration. Following the affine registration, a symmetric inverse consistent nonlinear registration algorithm based on mutual information as similarity measure [63] was used to co-register these images to the unbiased template described above.

For each MS brain, the JDs defined in the unbiased template space were obtained. Thus, in present study, the unbiased template served as the standard space for analyzing the relative volume differences between the groups. To compensate for the brain size differences among different subjects, the JD of each stripped brain was normalized by adjusting its mean to 1.0. The logarithmic of JD was used for the TBM analysis since it is more symmetric and is appropriate for classical statistical analysis [57].

2.5 Determination of gray matter atrophy and other MRI derived measures

As indicated above, anatomical structures in the MS brains were identified by mapping the parcellation associated with the MNI template to the unbiased template space. The left and right compartments of each of the GM structures are treated as a single structure in the MNI template. We followed this convention in the present study. The atrophy of GM structures was determined by calculating the mean value of the logarithmic of JD obtained in each individual image pair (MS and template) registration. The T2 hyperintense lesions were identified and segmented using the unified segmentation approach described elsewhere [69] on dual FSE and FLAIR images. The T1 hypointense lesions were segmented on the pre- and post-contrast T1-weighted images as described by [70]. Normalized CSF fraction was calculated as the ratio of CSF volume to the whole brain volume. The T2 and T1 lesion and normalized CSF fraction

masks were aligned with the 3D T1 images using 3D rigid body registration. The T2, T1 lesion and CSF masks were normalized with respect to the unbiased template following their alignment with 3D T1 images, to investigate their relation to regional atrophy in the GM structures.

In addition to determining the atrophy of GM structures, we also sought to determine the association between the regional atrophies with EDSS and various MRI-derived measures. We also wanted to determine the progression of atrophy with EDSS. Therefore, we divided the MS patients into two subgroups based on their EDSS: 0−3.5 and 4.0−6.5. The selection of the two cohorts was based on the apparent importance of EDSS 4.0; data from a variety of natural history and cross-sectional databases suggest that EDSS of 4 is associated with high rates of clinical disability, loss of independence and productivity, the onset of the progressive phase of the disease, and increased medical costs and societal burdens [71-73].

2.6 Analysis of atrophy of GM structures with EDSS

Statistical analysis of covariance (ANCOVA) was used to compare the volumes of GM structures among various groups (normal and MS subjects with EDSS 0; and two subgroups of MS subjects) with age and sex as nuisance covariates. Following ANCOVA analysis, two-sampled t-test for unpaired data was performed to compare the group differences. False-discovery rate (FDR = 0.05) was used to correct for multiple comparisons across the whole brain at each voxel. We have tested the effect of different cluster sizes (10, 20, 30, and 40) on the t-statistic maps and did not find any visual difference. Therefore, in all these studies, a cluster size of 10 was used.

Pearson correlation coefficients between the mean value of the logarithmic of JD of various GM structures and EDSS, T2 and T1 lesion loads, and normalized CSF were computed using MATLAB version 6.5.

3. Results

Figure 2 shows an example of nonlinear registration of an image at two different cross-sections with the unbiased template. The JDs, obtained from the deformation fields clearly demonstrate ventricular expansion and DGM atrophy. Figure 3 shows t-statistic color maps, obtained with TBM, showing the differences between MS patients (23 females, 3 males with a mean age of 40.2 ± 9.96 yrs) with EDSS of 0 (entirely normal neurologic examination) and normal subjects (10 females, 10 males; age range 41.2 ± 7.02 yrs). This analysis was based on ANCOVA with age and gender as nuisance covariates. The results demonstrate statistically significant atrophy in most of the GM structures in MS even in the absence of clinical disability.

To investigate the effect of clinical disability on atrophy, the 88 subjects were divided into two groups: group A comprises of 75 subjects with low EDSS (range 0−3.5) and the remaining 13 subjects with relatively high EDSS (≥4.0) were included in group B. The t-statistic color maps comparing these two groups, based on ANCOVA to account for the effect of age and gender, are shown in Fig. 4. As can be observed from this figure, while the atrophy increases in different structures at the higher EDSS strata, the effect of EDSS on thalamus appears to be particularly prominent. We have also performed two sample t-test without including gender and age as covariates and did not find any noticeable effect of gender and age on the t-statistic maps. Therefore, all the correlations we calculated without including age and gender as covariates.

The atrophy of three DGM structures that are found to be negatively correlated with EDSS are thalamus ($r = -0.51$, $p = 3.85\times10^{-7}$), caudate nucleus ($r = -0.43$, $p = 2.35\times10^{-5}$), and putamen ($r = -0.36$, $p = 6.12\times10^{-6}$). The scatter plots of regional atrophy of these structures against EDSS are shown in Fig. 5.

The regional atrophy of thalamus ($r = -0.56$, $p = 9.96\times10^{-9}$), caudate nucleus ($r = -0.31$, $p = 3.10\times10^{-3}$), and putamen ($r = -0.50$, $p = 6.06\times10^{-7}$) also correlated with the T2 hyperintense lesion load. Similarly, significant correlations between T1 hypointense lesion load and regional atrophy (thalamus: $r = -0.61$, $p = 2.29\times10^{-10}$; caudate nucleus: $r = -0.35$, $p = 9.51\times10^{-4}$; and putamen: $r = -0.43$, $p = 3.51\times10^{-5}$) were observed. nCSF, a measure of total brain atrophy, was also observed to correlate with DGM atrophy: thalamus ($r = -0.66$, $p = 3.55\times10^{-12}$), caudate nucleus ($r = -0.52$, $p = 2.31\times10^{-7}$), and putamen ($r = -0.66$, $p = 2.13\times10^{-12}$). The scatter plots of atrophy of these deep gray matter structures against the T2 and T1 lesion loads, and nCSF are shown in Figs. 6, 7 and 8. Table 2 summarizes significant correlations between atrophy of various GM structures with EDSS and MRI based measures.

4. Discussion

Earlier studies have investigated the atrophy of various GM structures and correlated with clinical disability, including cognitive deficits, and MRI-derived measures [29,31,43-45]. However, as described below, there are a number of methodological differences between the current and published studies. The use of unbiased template, as stated earlier, offers a robust estimation of atrophy measurements. As demonstrated in the previous studies [63] and briefly described below, the inverse consistent registration that we used for constructing the unbiased atlas is diffeomorphic. The deformation based parcellation of IBSR dataset [74] using this registration was shown to result in significantly higher Dice similarity indices compared to other methods such as ITK demons [67] and B-spline based deformation model [75]. The reported Dice similarity indices were 0.85, 0.83 and 0.78 for thalamus, putamen, and caudate nucleus [63] respectively. In addition, the validation studies based on the registration algorithm applied to MR brain images yielded an average inverse consistency error of 0.004 voxels with a maximum value less than 0.1 voxels.

To the best of our knowledge, this is the first study to use TBM for analyzing regional atrophy of GM structures in MS. The TBM based statistical analysis does not require segmentation of GM tissues and/or smoothing tissue maps that is required for VBM analysis. We believe that TBM analysis combined with the unbiased template based on accurate inverse consistent and diffeomorphic nonlinear registration has resulted in robust estimation of atrophy.

Similar to the other published study [30], we have demonstrated that many GM structures show atrophy in patients with modest or no measurable clinical disability, as assessed by EDSS. However, as the clinical disability worsens, only a few structures, particularly thalamus, show more severe atrophy. The results are similar to that reported by Audoin et al. [50], where the thalamus atrophy was observed to increase with disease progression over a period of time. These authors also reported that the rate of atrophy in thalamus correlated with changes in EDSS but they did not find correlation between thalamus atrophy and EDSS during the follow-up study.

Our findings of significant correlation of thalamus atrophy with EDSS is in agreement with the results reported by Houtchens et al. [29], but not with Ceccarelli et al. [44] and Prinster et al. [43] who did not observe any such correlation. However, our observed correlation of thalamus atrophy with T2 lesion load ($r = -0.57$, $p = 9.96\times10^{-9}$) is similar to that reported by [44]. Ceccarelli et al. [44] have reported correlation between atrophy and T2 lesion load in left thalamus ($r = -0.70$, $p < 0.001$) and right thalamus ($r = -0.81$, $p < 0.001$) on 26 relapsingremitting MS subjects. The higher correlation observed by Ceccarelli et al. [44] may be due to a number of factors. Our automatic T2 lesion classification on FSE and FLAIR is based on unified approach proposed by Sajja et al. [69] and atrophy measurements are based on TBM. Ceccarelli et al. [44] have classified lesions manually and used VBM for atrophy measurements. Also, the number of MS subjects (88) recruited for this study is relatively high

in comparison to the number of MS subjects of relapsing phenotype (26) included in the study performed by Ceccarelli et al. [44].

The DGM structures, such as caudate nucleus, thalamus, and putamen play important roles in motor, sensory and cognitive behaviors [29,31,45,76]. The regional atrophy of these structures in MS patients could result in visual, motor, sensory, and gait impairments [77]. Therefore, our observed correlation between atrophy of these structures and EDSS is not surprising. It is unclear whether the observed atrophy of GM structures is the result of direct neuronal injury or the result of WM damage. For example, based on direct histopathologic evidence, neuronal loss has been documented in thalamus [26,27]. Our observed correlation of atrophy of various DGM structures with T1 hypointense and T2 hyperintense lesions appears to suggest a link between WM damage and atrophy of these structures. Finally our observed correlation between atrophy of these DGM structures with whole brain atrophy (nCSF) is consistent with the results reported by Houtchens et al. [29].

In addition to thalamus, caudate nucleus, and putamen atrophy, we have observed atrophy of other GM structures that include septal nuclei, red nucleus, and middle occipital gyrus. The correlation between atrophy of these structures with clinical disability and MRI-derived measures is variable.

The present study employs sophisticated and robust image analysis techniques for calculating regional atrophy in various GM structures, and demonstrates correlation with various MR measures and EDSS. However, there are certain limitations to these studies. Many of the GM structures play an important role in cognition. In these studies, we have not performed neuropsychological tests. It would have been interesting to investigate the association between atrophy and cognitive deficits seen in MS. In this study, we divided patients into two groups, based on their EDSS scores at what may be a critical level where future accumulated disability becomes more linear (i.e. the typical stage of onset of the secondary progressive phase of the disease) [73]. The majority of our patients had relatively modest EDSS scores that perhaps limits from defining the complete trajectory of GM atrophy with EDSS. More patients with higher EDSS need to be included to define GM atrophy with disease progression. This requires much larger number of patients than what we have included in these studies.

The nonlinear registration used in the TBM analysis ignored WM lesions. Since the registration was performed on T1-weighted images where most lesions appear isointense (except for black holes), we believe that ignoring the WM lesions would not significantly affect our results. We are currently developing techniques that would include WM lesions in the TBM analysis.

The present study is based on the data acquired at a single research center with rigorous quality assurance procedures for acquisition and analysis. This level of attention may not be feasible in a larger clinical setting. Generalization of our results requires analysis of data acquired at different centers. Finally, these are cross sectional studies and future studies should include longitudinal design. In spite of theses limitations, we believe that our studies provide important information about the role of DGM atrophy in MS even at a relatively modest clinical disability.

Acknowledgments

This work is supported by the National Institutes of Health Grant EB002095 to PAN. We acknowledge Mr. Vipul Kumar Patel in acquiring the image data on 3 T Philips Intera scanner.

References

1. Lublin FD, Reingold SC. Defining the clinical course of multiple sclerosis: results of an international survey. Neurology 1996;46:907–11. [PubMed: 8780061]

2. Charcot J. Histologie de la sclerose en plaques. Gaz Hop (Paris) 1868;141:554–8.
3. Taylor E. Zur patologischen anatomie der mutliplen sklerose. Dtsch ZNervenheilkd 1892:1–26.
4. Dawson JW. The histology of multiple sclerosis. Trans R Soc (Edinb) 1916;50:517–740.
5. Bo L, Vedeler CA, Nyland HI, Trapp BD, Mork SJ. Subpial demyelination in the cerebral cortex of multiple sclerosis. J Neuropathol Exp Neurol 2003;62:723–32. [PubMed: 12901699]
6. Brink BPVRBL. The pathology of multiple sclerosis is location-dependent: no significant complement activation is detected in purely intracortical lesions. Journal of Neuropathol Exp Neurol 2005;64:147–55.
7. Peterson JW, Bö L, Mörk S, Chang A, Trapp BD. Transected neurites, apoptotic neurons, and reduced inflammation in cortical multiple sclerosis lesions. Ann Neurol 2001;50:389–400. [PubMed: 11558796]
8. Sharma R, Narayana PA, Wolinsky JS. Grey matter abnormalities in multiple sclerosis: proton magnetic resonance spectroscopic imaging. Mult Scler 2001;7:221–6. [PubMed: 11548980]
9. Kapeller P, McLean MA, Griffin CM, Chard D, Parker GJ, Barker GJ, Thompson AJ, Miller DH. Preliminary evidence for neuronal damage in cortical grey matter and normal appearing white matter in short duration relapsing-remitting multiple sclerosis: a quantitative MR spectroscopic imaging study. J Neurol 2001;248:131–8. [PubMed: 11284131]
10. Narayana PA, Wolinsky JS, Rao SB, He R, Mehta M. Multicentre proton magnetic resonance spectroscopy imaging of primary progressive multiple sclerosis. Mult Scler 2004;10(Suppl 1):S73–8. [PubMed: 15218814]
11. Chard DT, Griffin CM, McLean MA, Kapeller P, Kapoor R, Thompson AJ, Miller DH. Brain metabolite changes in cortical grey and normal-appearing white matter in clinically early relapsing-remitting multiple sclerosis. Brain 2002;125:2342–52. [PubMed: 12244090]
12. Sijens PE, Mostert JP, Oudkerk M, De Keyser J. (1)H MR spectroscopy of the brain in multiple sclerosis subtypes with analysis of the metabolite concentrations in gray and white matter: initial findings. Eur Radiol 2006;16:489–95. [PubMed: 16028056]
13. Ge Y, Grossman RI, Udupa JK, Babb JS, Kolson DL, McGowan JC. Magnetization transfer ratio histogram analysis of gray matter in relapsing-remitting multiple sclerosis. Am J Neuroradiol 2001;22:470–5. [PubMed: 11237968]
14. Audoin B, Ranjeva JP, Au Duong MV, Ibarrola D, Malikova I, Confort-Gouny S, Soulier E, Viout P, Ali-Cherif A, Pelletier J, Cozzone PJ. Voxel-based analysis of MTR images: a method to locate gray matter abnormalities in patients at the earliest stage of multiple sclerosis. J Magn Reson Imaging 2004;20:765–71. [PubMed: 15503338]
15. Dehmeshki J, Chard DT, Leary SM, Watt HC, Silver NC, Tofts PS, Thompson AJ, Miller DH. The normal appearing grey matter in primary progressive multiple sclerosis: a magnetisation transfer imaging study. J Neurol 2003;250:67–74. [PubMed: 12527995]
16. Bozzali M, Cercignani M, Sormani MP, Comi G, Filippi M. Quantification of brain gray matter damage in different MS phenotypes by use of diffusion tensor MR imaging. Am J Neuroradiol 2002;23:985–8. [PubMed: 12063230]
17. Rovaris M, Bozzali M, Iannucci G, Ghezzi A, Caputo D, Montanari E, Bertolotto A, Bergamaschi R, Capra R, Mancardi GL, Martinelli V, Comi G, Filippi M. Assessment of normal-appearing white and gray matter in patients with primary progressive multiple sclerosis: a diffusion-tensor magnetic resonance imaging study. Arch Neurol 2002;59:1406–12. [PubMed: 12223026]
18. Vrenken H, Pouwels PJ, Geurts JJ, Knol DL, Polman CH, Barkhof F, Castelijns JA. Altered diffusion tensor in multiple sclerosis normal-appearing brain tissue: cortical diffusion changes seem related to clinical deterioration. J Magn Reson Imaging 2006;23:628–36. [PubMed: 16565955]
19. Oreja-Guevara C, Rovaris M, Iannucci G, et al. Progressive gray matter damage in patients with relapsing-remitting multiple sclerosis: a longitudinal diffusion tensor magnetic resonance imaging study. Arch Neurol 2005;62:578–84. [PubMed: 15824256]
20. Poonawalla AH, Hasan KM, Gupta RK, Ahn CW, Nelson F, Wolinsky JS, Narayana PA. Diffusion-tensor MR imaging of cortical lesions in multiple sclerosis: initial findings. Radiology 2008;246:880–6. [PubMed: 18195384]
21. Bermel RA, Innus MD, Tjoa CW, Bakshi R. Selective caudate atrophy in multiple sclerosis: a 3D MRI parcellation study. Neuroreport 2003;14:335–9. [PubMed: 12634479]

22. Niepel G, Tench ChR, Morgan PS, Evangelou N, Auer DP, Constantinescu CS. Deep gray matter and fatigue in MS: a T1 relaxation time study. J Neurol 2006;253:896–902. [PubMed: 16525881]
23. Ge Y, Jensen JH, Lu H, Helpern JA, Miles L, Inglese M, Babb JS, Herbert J, Grossman RI. Quantitative assessment of iron accumulation in the deep gray matter of multiple sclerosis by magnetic field correlation imaging. Am J Neuroradiol 2007;28:1639–44. [PubMed: 17893225]
24. Inglese M, Park SJ, Johnson G, Babb JS, Miles L, Jaggi H, Herbert J, Grossman RI. Deep gray matter perfusion in multiple sclerosis: dynamic susceptibility contrast perfusion magnetic resonance imaging at 3T. Arch Neurol 2007;64:196–202. [PubMed: 17296835]
25. Sharma J, Zivadinov R, Jaisani Z, Fabiano AJ, Singh B, Horsfield MA, Bakshi R. A magnetization transfer MRI study of deep gray matter involvement in multiple sclerosis. J Neuroimaging 2006;16:302–10. [PubMed: 17032378]
26. Cifelli A, Arridge M, Jezzard P, Esiri MM, Palace J, Matthews PM. Thalamic neurodegeneration in multiple sclerosis. Ann. Neurol 2002;52:650–3. [PubMed: 12402265]
27. Wylezinska M, Cifelli A, Jezzard P, Palace J, Alecci M, Matthews PM. Thalamic neurodegeneration in relapsing-remitting multiple sclerosis. Neurology 2003;60:1949–54. [PubMed: 12821738]
28. Brass SD, Benedict RH, Weinstock-Guttman B, Munschauer F, Bakshi R. Cognitive impairment is associated with subcortical magnetic resonance imaging grey matter T2 hypointensity in multiple sclerosis. Mult Scler 2006;12:437–44. [PubMed: 16900757]
29. Houtchens MK, Benedict RH, Killiany R, Sharma J, Jaisani Z, Singh B, Weinstock-Guttman B, Guttmann CR, Bakshi R. Thalamic atrophy and cognition in multiple sclerosis. Neurology 2007;69:1213–23. [PubMed: 17875909]
30. Henry RG, Shieh M, Okuda DT, Evangelista A, Gorno-Tempini ML, Pelletier D. Regional Grey Matter Atrophy in Clinically Isolated Syndromes at Presentation. J Neurol Neurosurg Psychiatry 2008;79:1236–44. [PubMed: 18469033]
31. Bermel RA, Bakshi R, Tjoa C, Puli SR, Jacobs L. Bicaudate ratio as a magnetic resonance imaging marker of brain atrophy in multiple sclerosis. Arch Neurol 2002;59:275–80. [PubMed: 11843699]
32. Hasan KM, Halphen C, Boska MD, Narayana PA. Diffusion tensor metrics, T2 relaxation, and volumetry of the naturally aging human caudate nuclei in healthy young and middle-aged adults: possible implications for the neurobiology of human brain aging and disease. Magn Reson Med 2008;59:7–13. [PubMed: 18050345]
33. Roelcke U, Kappos L, Lechner-Scott J, Brunnschweiler H, Huber S, Ammann W, Plohmann A, Dellas S, Maguire RP, Missimer J, Radu EW, Steck A, Leenders KL. Reduced glucose metabolism in the frontal cortex and basal ganglia of multiple sclerosis patients with fatigue: A 18 F-fluorodeoxyglucose positron emission tomography study. Neurology 1997;48:1566–71. [PubMed: 9191767]
34. Pagani E, Rocca MA, Gallo A, Rovaris M, Martinelli V, Comi G, Filippi M. Regional brain atrophy evolves differently in patients with multiple sclerosis according to clinical phenotype. Am J Neuroradiol 2005;26:341–46. [PubMed: 15709132]
35. Sepulcre J, Sastre-Garriga J, Cercignani M, Ingle GT, Miller DH, Thompson AJ. Regional gray matter atrophy in early primary progressive multiple sclerosis: a voxel-based morphometry study. Arch Neurol 2006;63:1175–8. [PubMed: 16908748]
36. Mesaros S, Rovaris M, Pagani E, Pulizzi A, Caputo D, Ghezzi A, Bertolotto A, Capra R, Falautano M, Martinelli V, Comi G, Filippi M. A magnetic resonance imaging voxel-based morphometry study of regional gray matter atrophy in patients with benign multiple sclerosis. Arch Neurol 2008;65:1223–30. [PubMed: 18779427]
37. Sabatini U, Pozzilli C, Pantano P, Koudriavtseva T, Padovani A, Millefiorini E, Di Biasi C, Gualdi GF, Salvetti M, Lenzi GL. Involvement of the limbic system in multiple sclerosis patients with depressive disorders. Biol Psychiatry 1996;39:970–5. [PubMed: 9162210]
38. Charil A, Dagher A, Lerch JP, Zijdenbos AP, Worsley KJ, Evans AC. Focal cortical atrophy in multiple sclerosis: relation to lesion load and disability. Neuroimage 2007;34:509–517. [PubMed: 17112743]
39. Fisher E, Lee JC, Nakamura K, Rudick RA. Gray matter atrophy in multiple sclerosis: A longitudinal study. Ann Neurol 2008;64:255–65. [PubMed: 18661561]

40. Fisniku LK, Chard DT, Jackson JS, Anderson VM, Altmann DR, Miszkiel KA, Thompson AJ, Miller DH. Gray matter atrophy is related to long-term disability in multiple sclerosis. Ann Neurol 2008;64:1–8. [PubMed: 18626972]
41. Hua X, Leow AD, Lee S, et al. 3D characterization of brain atrophy in Alzheimer's disease and mild cognitive impairment using tensor-based morphometry. Neuroimage 2008;41:19–34. [PubMed: 18378167]
42. Bakshi R, Benedict RH, Bermel RA, Jacobs L. Regional brain atrophy is associated with physical disability in multiple sclerosis: semiquantitative magnetic resonance imaging and relationship to clinical findings. J Neuroimag 2001;11:129–136.
43. Prinster A, Quarantelli M, Orefice G, Lanzillo R, Brunetti A, Mollica C, Salvatore E, Morra VB, Coppola G, Vacca G, Alfano B, Salvatore M. Grey matter loss in relapsing–remitting multiple sclerosis: A voxel-based morphometry study. Neuroimage 2006;29:859–67. [PubMed: 16203159]
44. Ceccarelli A, Rocca MA, Pagani E, Colombo B, Martinelli V, Comi G, Filippi M. A voxel-based morphometry study of grey matter loss in MS patients with different clinical phenotypes. Neuroimage 2008;42:315–22. [PubMed: 18501636]
45. Pirko I, Lucchinetti CF, Sriram S, Bakshi R. Gray matter involvement in multiple sclerosis. Neurology 2007;68:634–42. [PubMed: 17325269]
46. Cutter GR, Baier ML, Rudick RA, Cookfair DL, Fischer JS, Petkau J, Syndulko K, Weinshenker BG, Antel JP, Confavreux C, Ellison GW, Lublin F, Miller AE, Rao SM, Reingold S, Thompson A, Willoughby E. Development of a multiple sclerosis functional composite as a clinical trial outcome measure. Brain 1999;122:871–82. [PubMed: 10355672]
47. Fischer JS, Rudick RA, Cutter GR, Reingold SC. The Multiple Sclerosis Functional Composite Measure (MSFC): an integrated approach to MS clinical outcome assessment. National MS Society Clinical Outcomes Assessment Task Force. Mult Scler 1999;5:244–50. [PubMed: 10467383]
48. Ashburner J, Friston KJ. Voxel-based morphometry—the methods. NeuroImage 2000;11:805–21. [PubMed: 10860804]
49. Good CD, Johnsrude IS, Ashburner J, Henson RN, Friston KJ, Frackowiak RS. Avoxel-based morphometric study of ageing in 465 normal adult human brains. NeuroImage 2001;14:21–36. [PubMed: 11525331]
50. Audoin B, Davies GR, Finisku L, Chard DT, Thompson AJ, Miller DH. Localization of grey matter atrophy in early RRMS: A longitudinal study. J Neurol 2006;253:1495–1501. [PubMed: 17093899]
51. Chung MK, Dalton KM, Davidoson RJ. Tensor-based cortical surface morphometry via weighted spherical harmonic representation. IEEE Trans. On Medical Imag 2008;27:1143–51.
52. Kim J, Avants B, Patel S, Whyte J, Coslett BH, Pluta J, Detre JA, Gee JC. Structural consequences of diffuse traumatic brain injury: a large deformation tensor-based morphometry study. Neuroimage 2008;39:1014–26. [PubMed: 17999940]
53. Whitford TJ, Grieve SM, Farrow TF, Gomes L, Brennan J, Harris AW, Gordon E, Williams LM. Volumetric white matter abnormalities in first-episode schizophrenia: a longitudinal, tensor-based morphometry study. Am J Psychiatry 2007;164:1082–9. [PubMed: 17606660]
54. Brambati SM, Renda NC, Rankin KP, Rosen HJ, Seeley WW, Ashburner J, Weiner MW, Miller BL, Gorno-Tempini ML. A tensor based morphometry study of longitudinal gray matter contraction in FTD. Neuroimage 2007;35:998–1003. [PubMed: 17350290]
55. Brambati SM, Rankin KP, Narvid J, Seeley WW, Dean D, Rosen HJ, Miller BL, Ashburner J, Gorno-Tempini ML. Atrophy progression in semantic dementia with asymmetric temporal involvement: A tensor-based morphometry study. Neurobiol Aging 2009;30:103–11. [PubMed: 17604879]
56. Hua X, Leow AD, Parikshak N, Lee S, Chiang MC, Toga AW, Jack CR Jr, Weiner MW, Thompson PM. The alzheimer's disease neuroimaging initiative. Tensor-based morphometry as a neuroimaging biomarker for Alzheimer's disease: An MRI study of 676 AD, MCI, and normal subjects. NeuroImage 2008;43:458–69. [PubMed: 18691658]
57. Leow AD, Klunder AD, Jack CR Jr. et al. Longitudinal stability of MRI for mapping brain change using tensor-based morphometry. NeuroImage 2006;31:627–40. [PubMed: 16480900]
58. Lepore N, Brun C, Chou YY, Chiang MC, Dutton RA, Hayashi KM, Luders E, Lopez OL, Aizenstein HJ, Toga AW, Becker JT, Thompson PM. Generalized tensor-based morphometry of HIV/AIDS using multivariate statistics on deformation tensors. IEEE Trans Med Imag 2008;27:129–41.

59. Joshi S, Davis B, Jomier M, Gerig G. Unbiased diffeomorphic template construction for computational anatomy. NeuroImage 2004;23:S151–60. [PubMed: 15501084]
60. Lepore N, Brun C, Pennec X, Chou YY, Lopez OL, Aizenstein HJ, Becker JT, Toga AW, Thompson PM. Mean template for tensor-based morphometry using deformation tensors. MICCAI 2007:826–33. [PubMed: 18044645]
61. Chung MK, Worsley KJ, Paus T, Cherif C, Collins DL. A unified statistical approach to deformation-based morphometry. Neuroimage 2001;14:595–606. [PubMed: 11506533]
62. Gaser C, Volz HP, Kiebel S, Riehemann S, Sauer H. Detecting structural changes in whole brain based on nonlinear deformations-application to schizophrenia research. Neuroimage 1999;10:107–13. [PubMed: 10417245]
63. Tao G, He R, Datta S, Narayana PA. Mutual information driven inverse consistent nonlinear registration. IEEE EMBC 2008:3957–60.
64. Polman CH, Reingold SC, Edan G, Filippi M, Hartung HP, Kappos L, Lublin FD, Metz LM, McFarland HF, O'Connor PW, Sandberg-Wollheim M, Thompson AJ, Weinshenker BG, Wolinsky JS. Diagnostic criteria for multiple sclerosis: 2005 revisions to the “McDonald Criteria”. Ann Neurol 2005;58:840–46. [PubMed: 16283615]
65. Marcus DS, Wang TH, Parker J, Csernansky JG, Morris JC, Buckner RL. Open access series of imaging studies (OASIS): cross-sectional MRI data in young, middle aged, nondemented, and demented older adults. Journal of Cognitive Neuroscience 2007;19:1498–1507. [PubMed: 17714011]
66. Ashburner J, Friston K. MRI sensitivity correction and tissue classification. NeuroImage 1998;7:S706.
67. Thirion JP. Image matching as diffusion process: an analogy with Maxwell's demons. Med. Imag. Anal 1998;2:243–60.
68. Christensen GE, Johnson HJ. Consistent image registration. IEEE Trans. on Med. Imag 2001;20:568–82.
69. Sajja BR, Datta S, He R, Mehta M, Gupta RK, Wolinsky JS, Narayana PA. Unified approach for multiple sclerosis lesion segmentation on brain MRI. Ann Biomed Eng 2006;34:142–51. [PubMed: 16525763]
70. Datta S, Sajja BR, He R, Wolinsky JS, Gupta RK, Narayana PA. Segmentation and quantification of black holes in multiple sclerosis. Neuroimage 2006;29:467–74. [PubMed: 16126416]
71. Casado V, Romero L, Gubieras L, Alonso L, Moral E, Martinez-Yelamos S, Martinez-Yelamos A, Carmona O, Arbizu T. An approach to estimating the intangible costs of multiple sclerosis according to disability in Catalonia, Spain. Mult Scler 2007;13:800–04. [PubMed: 17613609]
72. Confavreux C, Vukusic S, Adeleine P. Early clinical predictors and progression of irreversible disability in multiple sclerosis: an amnesic process. Brain 2003;126:770–82. [PubMed: 12615637]
73. Confavreux C, Vukusic S, Moreau T, Adeleine P. Relapses and progression of disability in multiple sclerosis. N Engl J Med 2000;343:1430–38. [PubMed: 11078767]
74. IBSR. Internet Brain Segmentation Repository (IBSR), the Center for Morphometric Analysis at Massachusetts General Hospital. MR brain images and their manual segmentations. 2007. http://www.cma.mgh.harvard.edu/ibsr/
75. Rueckert D, Sonoda LI, Hayes C, Hill DLG, Leach MO, Hawkes DJ. Non-rigid registration using free-form deformations: Application to breast MR images. IEEE Trans. on Med. Imag 1999;18:712–21.
76. Carone DA, Benedict RHB, Dwyer MG, Srinivasaraghavan B, Yella V, Abdelrahman N, Weinstock-Guttman B, Munschauer FE, Zivadinov R. Deep gray matter atrophy predicts cognitive impairment in multiple sclerosis. Neurology 2006;66(5 Suppl 2):A97.
77. Balcer LJ. Clinical outcome measures for research in multiple sclerosis. J Neuroophthalmology 2001;2:296–301.

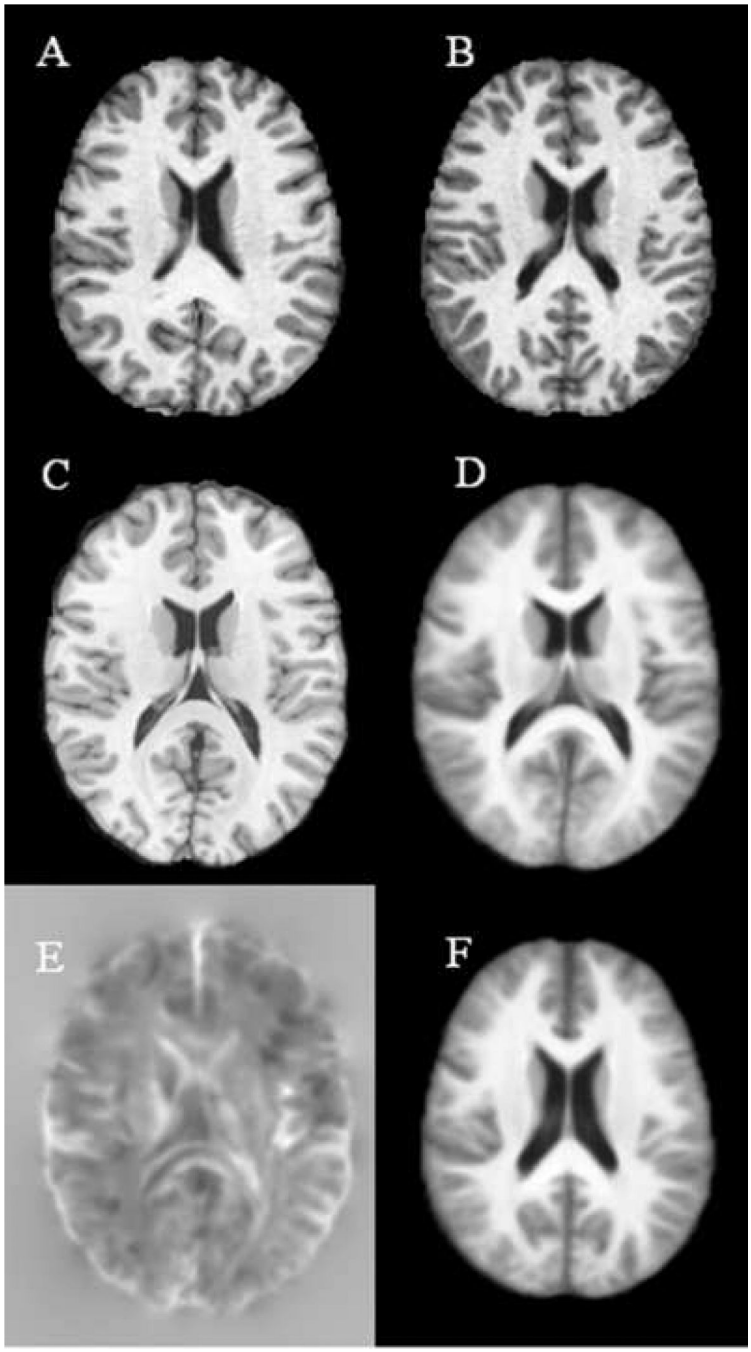

Fig. 1.

Creation of unbiased Template: Normal brain images obtained from OASIS datasets (A and B); (C) MNI template, Collin27; (D) average of 20 normal images in the MNI template space after inverse consistent nonlinear registration; (E) Jacobian determinant of the average of 20 transformations defined on MNI template; and (F) Intensity averaged unbiased template by mapping D through the inverse of the average geometrical deformations of the 20 nonlinear transformations.

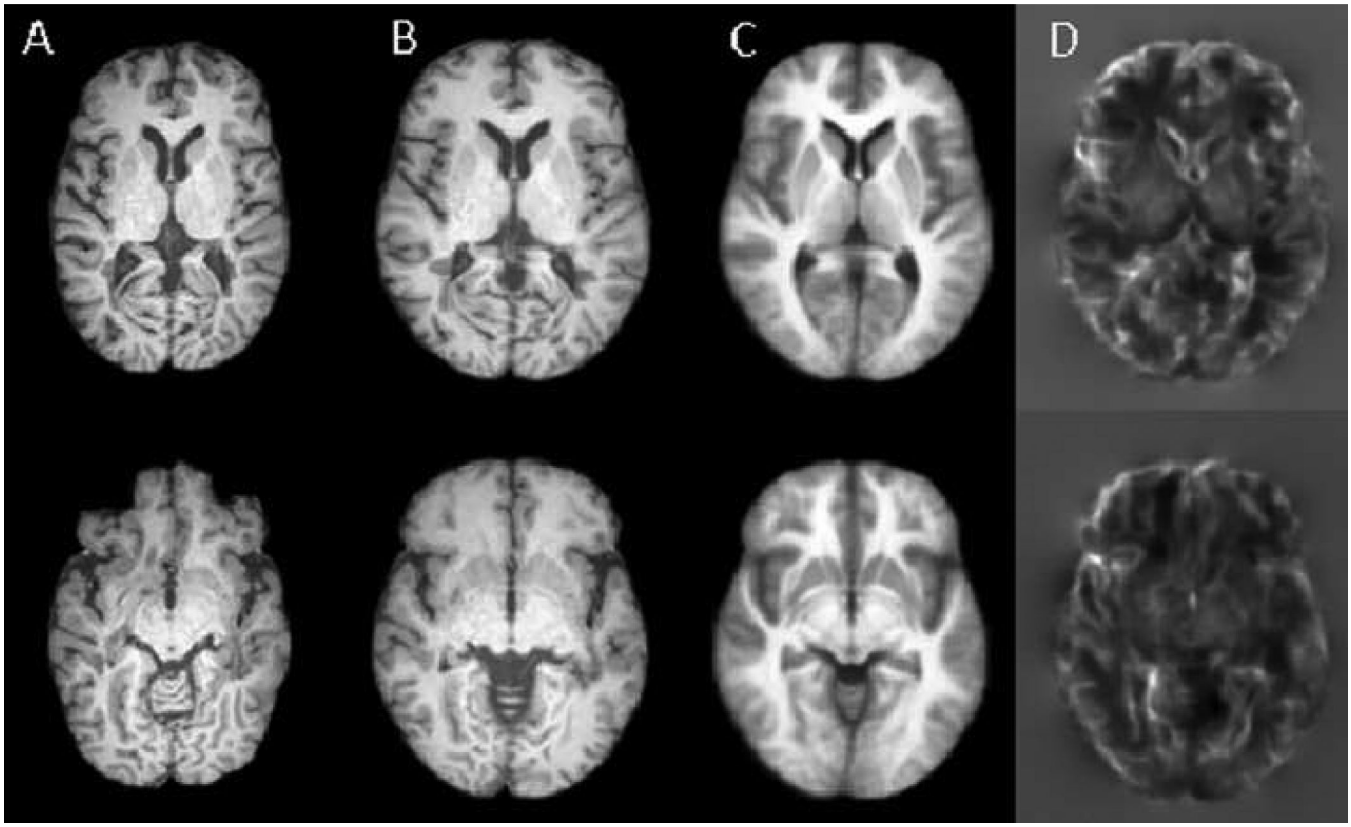

Fig. 2.
MRI brain images of an MS subject registered to the unbiased template: First column (A) Selected cross-sections of the source MS subject with EDSS 4.5; second column (B) MS images registered to the unbiased template; third column (C) Unbiased intensity averaged template; and fourth column (D) Jacobian maps in the unbiased template space.

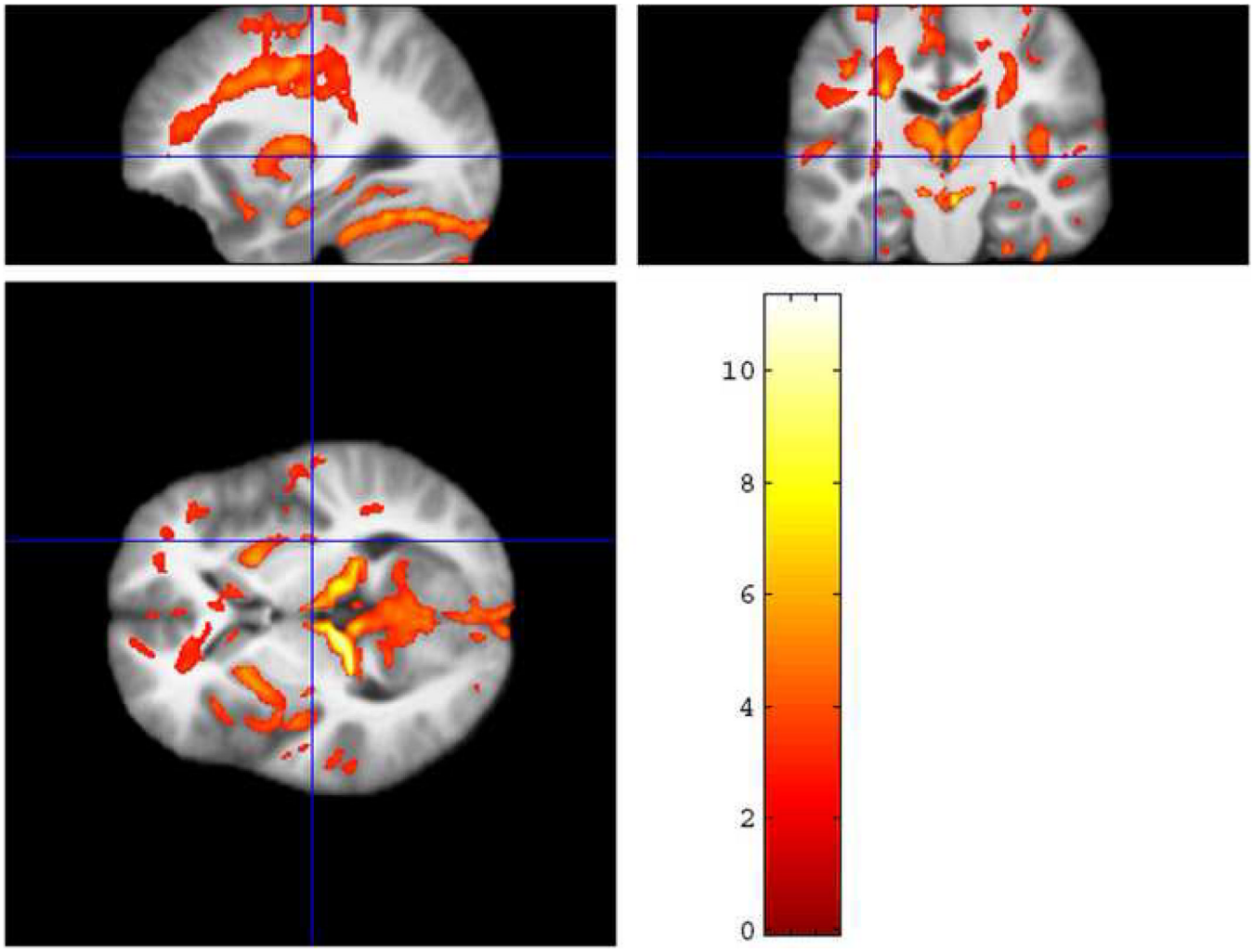

Fig. 3.

TBM results based on two sample t-test using ANCOVA between normal controls (10 males, 10 females; age 41.2 ± 7.02 yrs) and relapsing MS subjects (23 females, 3 males; age 40.2 ± 9.96 yrs) with EDSS = 0. The overlaid color area represents the regions with significant atrophy (FDR = 0.05) in the MS group with EDSS = 0 compared to the normal controls. The cluster size is 10.

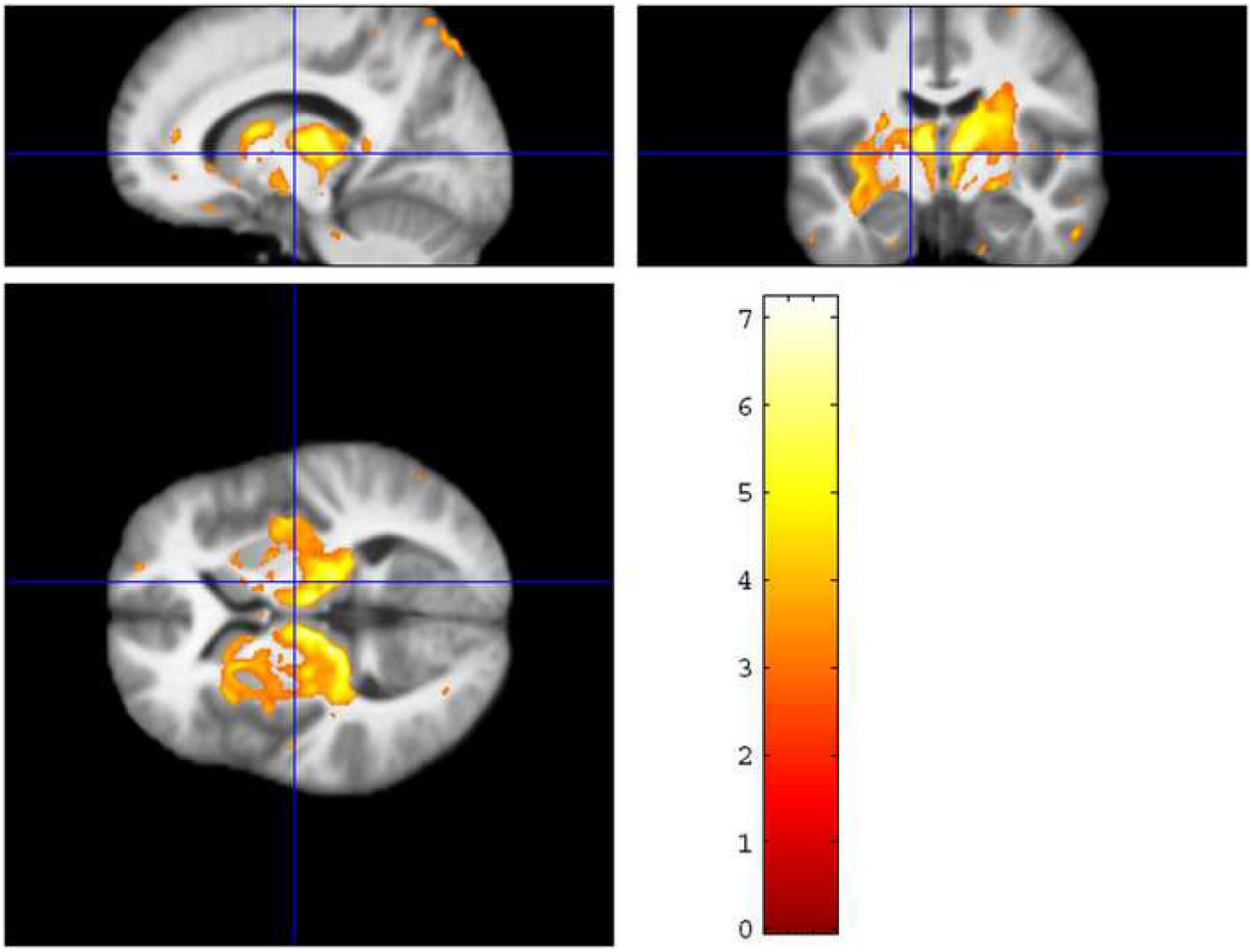

Fig. 4.
TBM results based on two sample t-test using ANCOVA between the two subgroups with EDSS ≤ 3.5 and EDSS ≥ 4.0 in the relapsing MS patients. The overlaid color map represents the regions with significant atrophy (FDR = 0.05) between these two subgroups. The cluster size is 10.

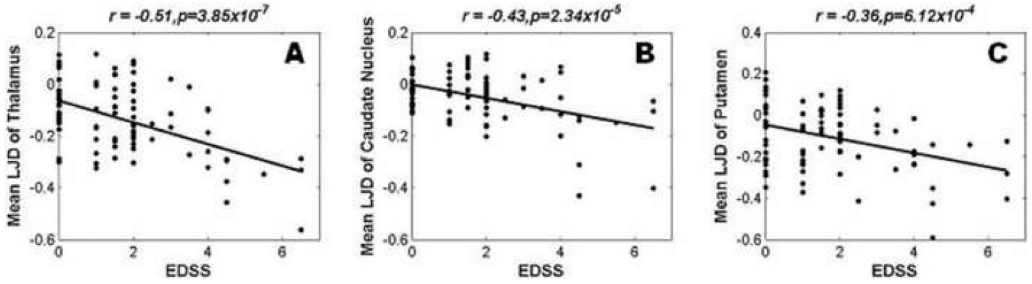

Fig. 5.

Correlation of mean logarithmic of Jacobian determinant with EDSS in 88 relapsing MS patients for (A) thalamus, (B) caudate nucleus, and (C) putamen.

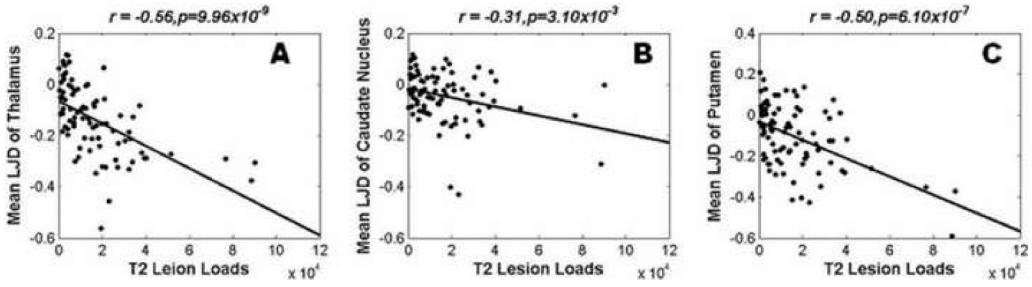

Fig. 6.

Correlation of mean logarithmic of Jacobian determinant with T2 lesion load in 88 relapsing MS patients for (A) thalamus, (B) caudate nucleus, and (C) putamen.

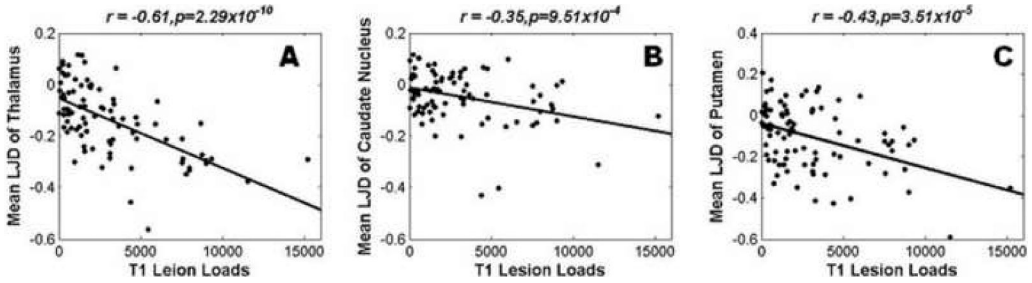

Fig. 7.

Correlation of mean logarithmic of Jacobian determinant with T1 hypointense lesion load in 88 relapsing MS patients for (A) thalamus, (B) caudate nucleus, and (C) putamen.

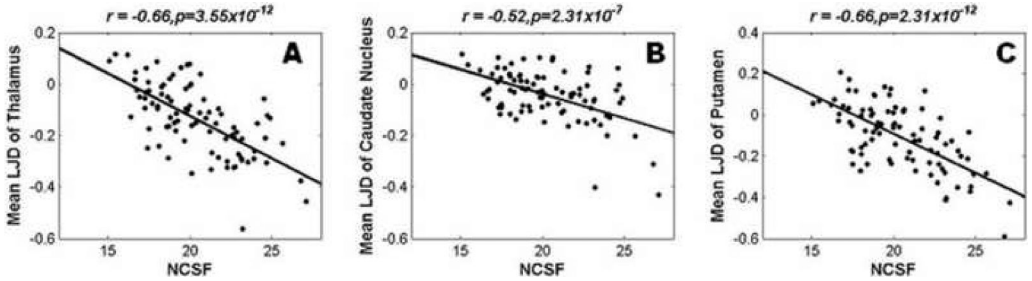

Fig. 8.

Correlation of mean logarithmic of Jacobian determinant with nCSF in 88 relapsing MS patients for (A) thalamus, (B) caudate nucleus, and (C) putamen.

Table 1

Frequency distribution of EDSS for all the 88 subjects.

EDSS	Number of Subjects
0	26
1.0−1.5	25
2−2.5	19
3−3.5	5
4−4.5	9
5−5.5	1
6−6.5	3

Table 2

The correlation (r, p) between atrophy of few gray matter (GM) structures with EDSS, T1 lesion loads, T2 lesions loads and nCSF.

GM Structures	EDSS	T2 Lesion Loads	T1 Lesion Load	NCSF
Thalamus	$-0.51, 3.85\times10^{-7}$	$-0.56, 9.96\times10^{-9}$	$-0.61, 2.29\times10^{-10}$	$-0.66, 3.55\times10^{-12}$
Caudate Nucleus	$-0.43, 2.35\times10^{-5}$	$-0.31, 3.10\times10^{-3}$	$-0.35, 9.51\times10^{-4}$	$-0.52, 2.31\times10^{-7}$
Putamen	$-0.36, 6.12\times10^{-4}$	$-0.50, 6.06\times10^{-7}$	$-0.43, 3.51\times10^{-5}$	$-0.66, 2.13\times10^{-12}$
Pons	$-0.29, 7.06\times10^{-3}$	–	$-0.21, 4.52\times10^{-2}$	$-0.30, 4.37\times10^{-3}$
Septal Nuclei	$-0.39, 1.75\times10^{-4}$	–	–	$-0.42, 4.15\times10^{-5}$
Red Nucleus	$-0.30, 4.55\times10^{-3}$	–	–	$-0.40, 1.18\times10^{-4}$
Middle Occipital Gyrus	$-0.28, 9.31\times10^{-3}$	–	–	$-0.20, 7.07\times10^{-2}$
Amygdala	–	$-0.45, 9.49\times10^{-6}$	$-0.28, 8.67\times10^{-3}$	$-0.38, 2.19\times10^{-4}$
Cingulate Gyrus	–	$-0.47, 4.37\times10^{-6}$	$-0.43, 3.04\times10^{-5}$	$-0.23, 3.32\times10^{-2}$
Middle Temporal Gyrus	–	$-0.33, 1.61\times10^{-3}$	$-0.34, 1.15\times10^{-3}$	–
Inferior Parietal Lobule	–	$-0.23, 2.97\times10^{-2}$	$-0.30, 3.92\times10^{-3}$	–
Entorhinal Area	–	$-0.34, 1.36\times10^{-3}$	$-0.23, 3.36\times10^{-2}$	–
Insular Cortex	–	$-0.25, 2.01\times10^{-2}$	–	$-0.30, 4.63\times10^{-3}$
Globus Pallidus Par Externa	–	–	–	$-0.37, 3.61\times10^{-4}$
Globus Pallidus Pars Interna	–	–	–	$-0.36, 6.71\times10^{-4}$
Middle Fronto-orbital	–	–	–	$-0.36, 6.85\times10^{-4}$